

Weak lensing and dark energy: the impact of dark energy on nonlinear dark matter clustering

Shahab Joudaki, Asantha Cooray

Center for Cosmology, Dept. of Physics & Astronomy, University of California, Irvine, CA 92697

Daniel E. Holz

Theoretical Division, Los Alamos National Laboratory, Los Alamos, NM 87545

(Dated: August 24, 2018)

We examine the influence of percent-level dark energy corrections to the nonlinear matter power spectrum on constraints of the dark energy equation of state from future weak lensing probes. We explicitly show that a poor approximation (off by $\gtrsim 10\%$) to the nonlinear corrections causes a $\gtrsim 1\sigma$ bias on the determination of the dark energy equation of state. Future weak lensing surveys must therefore incorporate dark energy modifications to the nonlinear matter power spectrum accurate to the percent-level, to avoid introducing significant bias in their measurements. For the WMAP5 cosmology, the more accurate power spectrum is more sensitive to dark energy properties, resulting in a factor of two improvement in dark energy equation of state constraints. We explore the complementary constraints on dark energy from future weak lensing and supernova surveys. A space-based, JDEM-like survey measures the equation of state in five independent redshift bins to $\sim 10\%$, while this improves to $\sim 5\%$ for a wide-field ground-based survey like LSST. These constraints are contingent upon our ability to control weak lensing systematic uncertainties to the sub-percent level.

I. INTRODUCTION

The images of distant galaxies are gravitationally lensed by matter inhomogeneities along the line-of-sight. In the weak lensing regime these percent-level magnifications and shape distortions of galaxies need to be analyzed statistically (see [1, 2] for a review). By extracting the shear power spectrum of weakly lensed sources [3–8], the nature of the dark energy has been constrained with lensing surveys [7, 8].

In a comprehensive analysis of future dark energy probes by the Dark Energy Task Force (DETF), weak lensing is singled out as particularly promising, in comparison with supernovae (SNe), galaxy cluster counting, and baryon acoustic oscillations (BAOs) [9]. An important aspect is that the lensing power spectrum depends on both the lensing kernel and the matter power spectrum, making lensing a powerful probe of both background cosmology and the growth of structure.

The optimism associated with lensing is predicated on overcoming the vast systematic uncertainties in both measurement and in theory [10–22]. These systematics include dark energy corrections to the modeling of the nonlinear matter power spectrum [18, 19], higher order correction terms in the lensing integral (such as due to the Born approximation and lens-lens coupling [20–22]), and uncertainties of the matter power spectrum on nonlinear scales due to the strong influence of baryonic physics [14–17]. Observational systematics include photometric redshift uncertainties, multiplicative factors in shear due to calibration errors, and additive factors due to PSF anisotropies [10, 11].

Furthermore, the observed ellipticities of weakly lensed galaxies are sensitive to the reduced shear,

$g = \gamma/(1 - \kappa)$, where γ is the shear and κ is the convergence. In the weak lensing regime we make use of the expansion of the reduced shear to first order in the fields: $g \approx \gamma$. For future lensing surveys, this approximation induces a bias on the cosmological parameters at the same order as that of the parameter constraints [23, 24]. For current purposes, however, we continue to make use of this simplifying assumption of the shear as the lensing observable.

In this work we examine one particular lensing systematic: dark energy corrections to the nonlinear matter power spectrum, and the impact of these on dark energy constraints from the weak lensing power spectrum. We utilize two approaches towards modeling the nonlinear matter power spectrum in an evolving equation of state (EOS) environment. Both approaches are based upon the Smith et al. (2003) [25] prescription, valid for $w = -1$. The conventional route in computing the matter power spectrum for $w(z) \neq -1$ has been to use the $w = -1$ fitting functions of Smith et al. with appropriate modifications to the growth function and the redshift dependence of the matter density. We compare this method to that developed by McDonald, Trac, & Contaldi (2006) [19] for a constant w cosmology, where numerical simulations underlie a fitting scheme that provides corrections to the Smith et al. results. This latter approach approximates the dependence of the matter power spectrum on a constant dark energy EOS to the level of a few percent. We further analyze measurements of the dark energy EOS in (decorrelated) redshift bins, as well as direct measurements of a two-parameter Taylor expansion form for the EOS.

Our calculational methods are described in Section 2, with a basic review of the computation of distances, the growth function, the nonlinear matter

power spectrum, and the weak lensing power spectrum. In Section 3, we provide the dark energy constraints from weak lensing tomography, utilizing two different approaches for calculating the nonlinear matter power spectrum in a $w(z) \neq -1$ cosmology. We examine the complementarity between future weak lensing surveys and expansion history probes (e.g. supernovae distances measurements at $z < 1.8$). We also discuss the bias in dark energy due to uncertainties in the nonlinear matter power spectrum. At the end of Section 3 we provide an exploration of constraint contamination due to observational systematic uncertainties. Section 4 concludes with a discussion of our findings. We take our fiducial cosmological model, in accordance with WMAP5 data, to be a flat Λ CDM universe with $\Omega_c = 0.215$, $\Omega_b = 0.045$, $h = 0.72$, $n_s = 0.96$, $\sigma_8 = 0.8$, and no massive neutrinos [26].

II. CALCULATIONAL METHOD

We begin with a summary of our calculation. We briefly describe our cosmological distance and growth function, and then discuss the relevant observational quantities for weak lensing.

A. Distances

The comoving distance to an object at redshift z is

$$\chi(z) = \frac{1}{\sqrt{|\Omega_k|}H_0} X \left(\sqrt{|\Omega_k|} \int_0^z \frac{dz'}{H(z')/H_0} \right), \quad (1)$$

where $X(x) = \sin(x)$ for a closed universe, $\sinh(x)$ for an open universe, and x for a flat universe, and where $H_0 = 100 h \text{ km s}^{-1} \text{ Mpc}^{-1}$ is the Hubble constant. The Hubble parameter is given by

$$H(z) = H_0 \sqrt{\Omega_m(1+z)^3 + \Omega_w F(z) + \Omega_k(1+z)^2}, \quad (2)$$

where $\{\Omega_m, \Omega_w, \Omega_k\}$ are the present matter, dark energy, and curvature densities, in units of the critical density. The evolution of the dark energy is represented by $F(z)$. For a cosmological constant, $F(z) \equiv 1$.

We parameterize the evolution of the dark energy in two distinct ways. We use a popular Taylor expanded form for the dark energy EOS, given by $w(z) = w_0 + z/(1+z)w_a$ [27], from which one obtains $F(z) = (1+z)^{3(1+w_0+w_a)} e^{-3w_a \frac{z}{1+z}}$. Alternatively, instead of assuming a particular (physically unmotivated) model for the EOS, we utilize an agnostic, model-free approach to the redshift evolution of the dark energy [29–32]. We fit for $w(z)$ binned in redshift:

$$w(z) = \sum_{i=1}^N w_i \Xi(z_i, z_{i+1}), \quad (3)$$

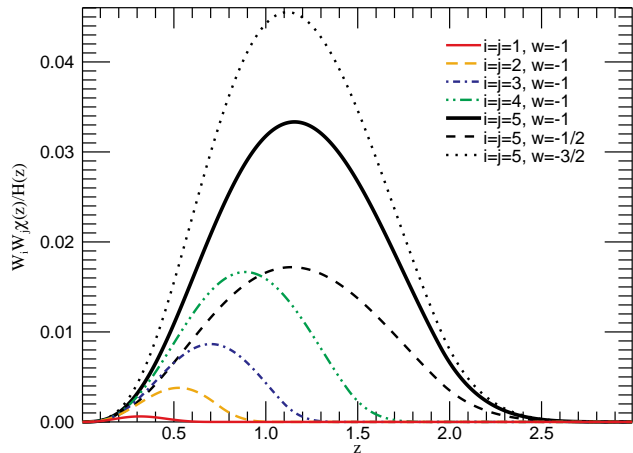


FIG. 1. Geometric factor, $W_i(z)W_j(z)\chi(z)/H(z)$, of five tomographic bins for our fiducial model ($w = -1$). For the fifth bin we also plot the kernel for $w = -1/2$ and $w = -3/2$. The narrowing of the lensing kernel for $w > -1$ stems from the decrease of each term with increasing w .

where $\Xi(z_i, z_{i+1})$ is a tophat function in the region spanned by $\{z_i, z_{i+1}\}$, but the ensuing analysis decorrelates the redshift bins. For this model-independent parameterization of the EOS,

$$F(z_{n-1} < z < z_n) = (1+z)^{3(1+w_n)} \prod_{i=0}^{n-1} (1+z_i)^{3(w_i - w_{i+1})}. \quad (4)$$

B. Growth Function

For a particular parameterization of the EOS one can calculate the growth of matter fluctuations in the universe. For matter perturbations on linear scales, it is possible to separate out the time evolution of the perturbation: $\delta(\mathbf{k}, z)/\delta(\mathbf{k}, 0) = D(z)/D(0)$, where $D(z)$ is the growth function (which evolves as the scale factor in a matter dominated universe). For $w(z) \neq -1$ this linear approximation breaks down on very large scales due to clustering in the dark energy. However, due to the large uncertainties from cosmic variance at these scales, the impact of dark energy inhomogeneities are negligible for weak lensing studies (e.g. [18, 33]).

The normalized growth function, $G(z) = (1+z)D(z)$, can be found by solving a second-order differential equation [34]:

$$G'' + \left[\frac{7}{2} - \frac{3}{2} \frac{w(a)\Omega_w(a)}{\Omega_m(a) + \Omega_w(a)} \right] \frac{G'}{a} + \frac{3}{2} \left[\frac{\Omega_w(1-w(a))}{\Omega_m(a) + \Omega_w(a)} \right] \frac{G}{a^2} = 0. \quad (5)$$

This differential equation is valid for non-flat geometries, and carries the initial conditions $\{G(z_{\text{md}}) = 1; \frac{dG}{dz}|_{z_{\text{md}}} = 0\}$ in a matter dominated epoch z_{md} .

C. Weak Lensing Observables

We employ weak lensing tomography, wherein we divide the redshift distribution of source galaxies into distinct redshift bins [35]. This provides information about the redshift distribution of the intervening lenses, and thereby allows for more stringent constraints on cosmological parameters [10, 35].

The number density of source galaxies in a square arcminute in each tomographic redshift bin (with boundaries $z_i < z_s < z_{i+1}$) is defined by $\bar{n}_i = \int_{z_i}^{z_{i+1}} dz_s \rho(z_s)$, where $\rho(z_s) = \bar{n}_g \frac{z_s^\alpha}{2z_0^\beta} e^{-(z_s/z_0)^\beta}$ is the redshift distribution of source galaxies [3]. We adopt $\{z_0 = 0.5, \alpha = 2, \beta = 1\}$ [36], appropriate for the Large Synoptic Survey Telescope (LSST [37, 38]), normalized such that $\int_0^\infty dz \rho(z) = \bar{n}_g$. We use the same distribution to describe our Joint Dark Energy Mission (JDEM) source population, but with improved \bar{n}_g (see Table I). We use the Born approximation, and perform the lensing calculation along the unperturbed photon path [20–22]. The lensing weight function of the i^{th} tomographic bin is given by

$$W_i(z) = \frac{3 \Omega_m H_0^2}{2 \bar{n}_i} (1+z) \chi(z) \times \int_{\max(z, z_i)}^{z_{i+1}} dz_s \frac{\chi(x(z_s) - x(z))}{\chi(z_s)} \rho(z_s), \quad (6)$$

for $z \leq z_{i+1}$, where $x(z) = \sqrt{|\Omega_k|} \int_0^z \frac{dz'}{H(z')/H_0}$. To ensure that we have no lenses behind our sources, we take $W_i(z) = 0$ for $z > z_{i+1}$. The weight function increases for a more negative dark energy equation of state, as shown in Figure 1. The power spectrum of the convergence field is subsequently given by the Limber approximation [39]:

$$C_{ij}(l) = \frac{2\pi^2}{l^3} \int_0^{z_H} dz \frac{W_i(z) W_j(z) \chi(z)}{H(z)} \Delta_{\text{NL}}^2(l/\chi(z), z), \quad (7)$$

where z_H is the horizon redshift, and $\Delta_{\text{NL}}^2(l/\chi(z), z)$ is the full nonlinear matter power spectrum.

For $l \gtrsim 300$, the dominant contribution to the matter power spectrum will be from nonlinear scales [40–42], emphasizing the need to correctly model the effect of dark energy at these scales. The observed convergence power spectrum, which is identical to that of the shear [2], is contaminated by shot noise due to the finite source density, as well as uncertainty in the intrinsic shapes of the source galaxies, leading to: $\hat{C}_{ij}(l) = C_{ij}(l) + \delta_{ij} \langle \gamma^2 \rangle / \bar{n}_i$ (which assumes that the noise is uncorrelated between tomographic bins). Whereas cosmic variance dominates the error on large angular scales, the shot noise is dominant on small scales.

For simplicity we take the intrinsic shape uncertainty of the source galaxies to be redshift independent: $\langle \gamma^2 \rangle^{1/2} = 0.22$, in accordance with expected results from a future ground-based survey such as

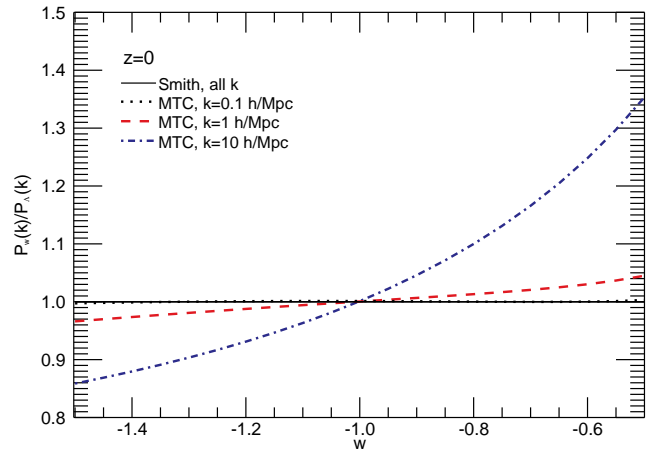


FIG. 2. Ratio of the present matter power spectrum of a constant dark energy EOS to that of a cosmological constant, $\Delta_w^2(k, z)/\Delta_\Lambda^2(k, z)$, as a function of w . The solid line is obtained by modifying the growth function and matter density evolution based on the Smith et al. prescription, while the other (more accurate) curves utilize the MTC corrections to the power spectrum.

LSST [36, 37]. We assume that the survey covers half of the sky, with a galaxy density of $\bar{n}_g = 50$ arcmin $^{-2}$ [36, 37]. For comparison, we also consider a space-based survey, such as a JDEM candidate like the SuperNova Acceleration Probe (SNAP) [43–45]. For simplicity, we keep the same source distribution and intrinsic shear uncertainty, modifying the source density to twice that of the ground-based survey, and the width of the survey to a tenth of the sky. The characteristics of the two surveys are summarized in Table I.

D. Nonlinear Matter Power Spectrum

We now detail our calculation of the matter power spectrum for a general dark energy cosmology.¹ In the linear regime the transfer function $T(k, z)$ is computed using the prescription of Eisenstein & Hu (1997) [47]. The dimensionless linear power spectrum, normalized to the variance of the matter density field on scales of $8 h^{-1}$ Mpc, σ_8 , is given by

$$\Delta_L^2(k, z) = k^{3+n_s} T^2(k, z) \frac{D^2(z)}{D^2(0)} \left(\frac{\sigma_{8,\text{obs}}}{\sigma_{8,\text{theory}}} \right)^2, \quad (8)$$

¹ We do not pursue a direct halo-model approach [46] for modeling the weak lensing power spectrum, since for the case of general dark energy models we have inadequate descriptions for the halo mass function, the halo dark matter profile, and the large-scale halo bias.

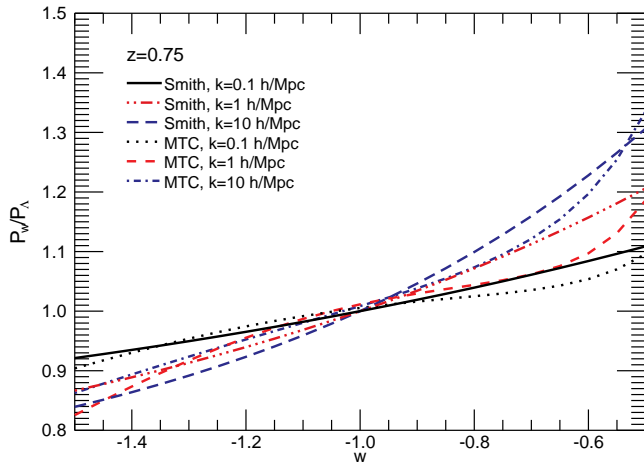


FIG. 3. Ratio of the matter power spectrum of a constant dark energy EOS to that of a cosmological constant, at $z=0.75$.

where n_s is the spectral index, $\sigma_{8,\text{obs}} = 0.8$, and

$$\sigma_{8,\text{theory}} = \sqrt{\int d \ln k \Delta_L^2(k, 0) J^2(8k')}, \quad (9)$$

with the spherical tophat filter, $J(8k') = [3/(8k')^3][\sin(8k') - (8k') \cos(8k')]$, and $k' = k h^{-1}$ Mpc is dimensionless. One can subsequently extend this power spectrum to nonlinear scales by calculating the appropriate effective spectral index, effective spectral curvature, and nonlinear scale, employing the fitting functions provided in Smith et al. [25].

The underlying cosmology in the Smith et al. fitting functions manifests itself in two distinct ways. First, cosmology impacts the evolution of the matter density, $\Omega_m(z)$, and the evolution of the growth of matter perturbations, $D(z)$. Second, cosmology fixes the functional form and coefficients associated with the fitting functions, which are fine-tuned to a suite of Λ CDM N-body simulations. Thus, whereas an arbitrary dark energy EOS could make an imprint on the matter power spectrum via its influence on $\Omega_m(z)$ and $D(z)$, the cosmological dependence of the N-body fitting functions remain fine-tuned to a $w \equiv -1$ dark energy EOS. A correct approximation of the matter power spectrum in an evolving EOS cosmology therefore requires both an update of the effective spectral parameters of the Smith et al. prescription, and a generalization of the fitting functions.

Probe	f_{sky}	\bar{n}_g (arcmin $^{-2}$)	z_{peak}	$\sqrt{\langle \gamma^2 \rangle}$
LSST	0.5	50	1.0	0.22
JDEM	0.1	100	1.0	0.22

TABLE I. Descriptions of our fiducial ground-based (LSST) and space-based (JDEM) probes.

No. of bins	z_1	z_2	z_3	z_4	z_5
1 bin	3.0	—	—	—	—
2 bins	1.3	3.0	—	—	—
3 bins	1.0	1.6	3.0	—	—
4 bins	0.85	1.3	1.85	3.0	—
5 bins	0.75	1.1	1.45	1.95	3.0

TABLE II. Redshift bins of the source distribution. The redshifts are determined such that each tomographic bin contains roughly the same number density of galaxies. We ignore sources above $z = 3$.

A full calculation of the matter power spectrum will thus require a large suite of N-body simulations. An alternative approach devised by McDonald, Trac, & Contaldi (2006; hereafter MTC) notes that many numerical uncertainties cancel when taking the ratios of power spectra [19]. By interpolating the matter power spectrum ratios between constant EOS values, MTC provide a route to a fast calculation of the nonlinear matter power spectrum in constant w cosmologies. An accurate matter power spectrum can thereby be obtained by computing the power spectrum for a Λ CDM universe, and subsequently multiplying it by a cosmology-dependent correction factor. In particular,

$$\Delta_{\text{NL},w}^2(k, z) = \Delta_{\text{NL},\Lambda}^2(k, z) \times \frac{D^2(z, w)/D^2(0, w)}{D^2(z, \bar{w})/D^2(0, \bar{w})} \Upsilon(k, z, \mathbf{p}), \quad (10)$$

where the N cosmological parameters are given by $\mathbf{p} = \{\Omega_m, \Omega_b, h, \sigma_8, n_s, w\}$, $\bar{w} \equiv -1$, and

$$\Upsilon(k, z, \mathbf{p}) = e^{\left(\prod_{i=1}^N \sum_{\nu_i=0}^M p_i^{\nu_i}\right) A_{\nu_1 \nu_2 \dots \nu_N}(k)}. \quad (11)$$

In this equation, M is the polynomial order of the parameters, and the coefficients $A_{\nu_1 \nu_2 \dots \nu_N}(k)$ are provided by a least squares fit to the MTC simulations.

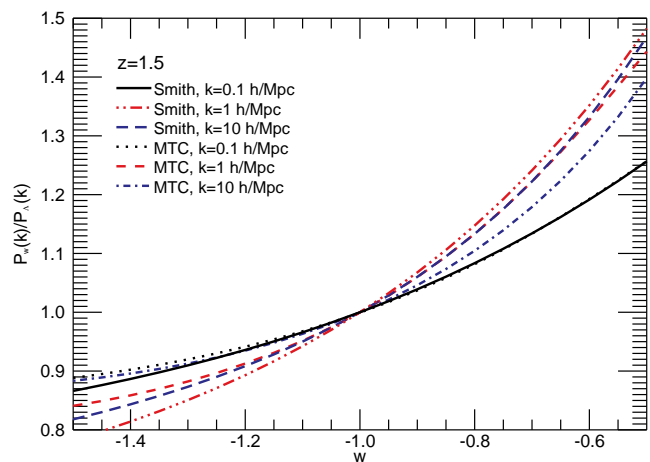


FIG. 4. Ratio of the matter power spectrum of a constant dark energy EOS to that of a cosmological constant, at $z=1.5$.

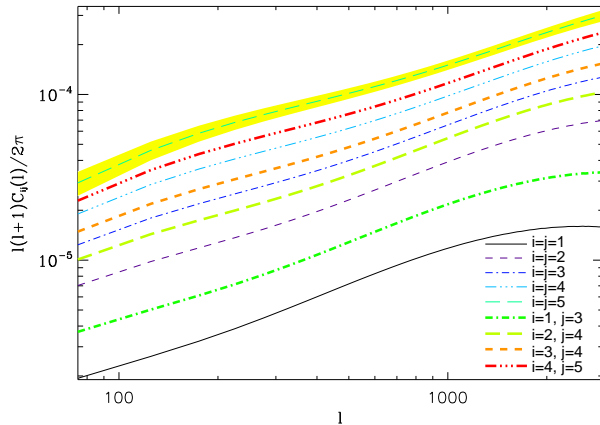


FIG. 5. Convergence power spectra for the case of five tomographic bins in a Λ CDM cosmology. We also include a number of representative cross-terms. For the $i = j = 5$ case, we include the noise contribution as a band about the curve.

On large scales the correction factor is equal to unity, as expected. The power spectrum ratios are only provided up to $z = 3/2$ and $k = 10 h \text{ Mpc}^{-1}$. However, since we only consider multipoles up to $l = 3000$, scales smaller than $k = 10 h \text{ Mpc}^{-1}$ are only probed at very low redshift, where the number density of sources becomes negligible. Moreover, as gradually smaller scales become linear with increasing redshift, for a fixed range of scales, the influence of dark energy on the matter power spectrum is progressively modelled by linear theory as the redshift increases. The dark energy correction factor for the matter power spectrum therefore covers an adequate range of scales and redshifts for weak lensing studies. Furthermore, as the MTC simulations have only been carried out for a limited range of parameter space, we have ensured that all of the cosmological parameters under consideration here live within their explored region.

III. RESULTS

We next explore the differences between the Smith et al. and MTC matter power spectra, and their respective impacts on cosmological constraints from future weak lensing probes. Systematic uncertainties are discussed in Section G.

A. Matter Power Spectrum: MTC vs. Smith

In Figures 2–4 we show the evolution of the MTC nonlinear matter power spectrum as a function of dark energy EOS (for constant w). Each figure represents a different redshift ($z = 0, 0.75, \text{ and } 1.5$), and every plot shows three different MTC curves, corresponding

to scales of $k = [0.1, 1.0, 10] h \text{ Mpc}^{-1}$. The curves are normalized to the power spectrum corresponding to a pure cosmological constant, and the Smith et al. fit (modifying solely the growth function and the matter density in accordance with the dark energy EOS) is also shown, for comparison. The MTC power spectra show large ($\gtrsim 10\%$) deviations from the simplified Smith et al. approximation over a range of reasonable w values. In general, constant $w < -1$ models lead to a suppression of the matter power spectrum as compared to that in a Λ CDM universe, with the suppression more pronounced at smaller (nonlinear) scales. Conversely, the matter power spectrum is enhanced for $w > -1$. As expected, the MTC correction factor becomes less pronounced at higher redshift as increasingly smaller scales become linear.

B. Weak Lensing

The convergence power spectrum depends on both the geometric factor, $W_i(z)W_j(z)\chi(z)/H(z)$, and the matter power spectrum, $\Delta^2(k, z)$, but in a competing manner. Whereas a decreasing dark energy EOS has the effect of increasing the geometric factor, and therefore the convergence power spectrum, it also suppresses the nonlinear matter power spectrum, which in turn suppresses the convergence power spectrum. As a result, these two effects partially cancel, thereby decreasing the sensitivity of weak lensing to dark energy.

In Figure 5 we plot the power spectrum of the convergence for five tomographic bins (with the redshift divisions listed in Table II), as well as some representative convergence power spectra cross-terms (e.g., between bins 4 and 5). We divide the power spectrum by its noise, $\Delta C_{ij}(l) = f_{\text{sky}}^{-1/2} \sqrt{2/(2l+1)}(C_{ij}(l) +$

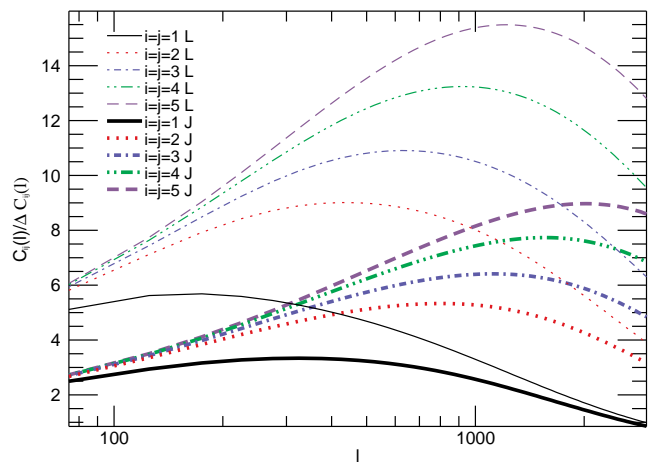


FIG. 6. Signal to noise with five tomographic bins in a Λ CDM cosmology, for LSST (denoted by ‘L’) and JDEM (‘J’).

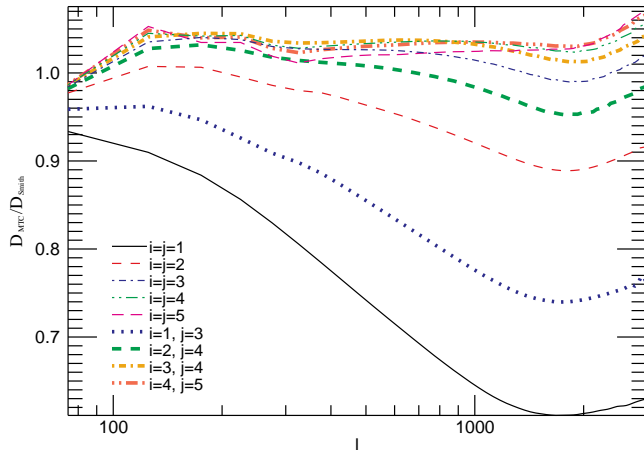


FIG. 7. Ratio of MTC to Smith et al. convergence spectra derivatives with respect to w , i.e. $D_{\text{MTC}}/D_{\text{Smith}} = \frac{\partial \mathbf{C}}{\partial w}|_{\text{MTC}} / \frac{\partial \mathbf{C}}{\partial w}|_{\text{Smith}}$.

$\delta_{ij} \langle \gamma^2 \rangle / \bar{n}_i$), in Figure 6. The signal to noise is consistently higher for the wider LSST than it is for the deeper JDEM. The larger width of LSST gives strong signal to noise in particular at smaller multipoles, while the greater depth of a JDEM-type survey makes it increasingly competitive at larger multipoles.

Figure 7 presents the ratio of the convergence spectra derivatives with respect to a constant EOS between Smith et al. and MTC. The MTC derivatives approach the Smith et al. derivatives in higher-redshift tomographic bins, as the corresponding matter power spectra converge at large redshift. This is because the MTC correction factor approaches unity at high z (see Figs. 2–4), and we therefore impose the approximation $\Delta^2(k, z)|_{\text{MTC}} \equiv \Delta^2(k, z)|_{\text{Smith}}$ for $z > 1.5$. Tables III and V show that our conclusions are insensitive to this approximation. The $z < 1.5$ entries in these tables are for five tomographic bins, with redshift divisions at $[0.59, 0.83, 1.04, 1.26, 1.5]$, engineered to preserve an equal number density of sources across each bin. Since the MTC derivatives have decreased relative to the Smith et al. ones, one might conclude that the sensitivity to dark energy has also decreased. However, due to the particular nature of the cross-correlations between cosmological parameters, this turns out not to be the case for our fiducial cosmology, as is shown below.

C. Constraints on Dark Energy

In the previous subsections we have examined the corrections to the nonlinear matter power spectrum due to the presence of dark energy. We now explore how these corrections impact weak lensing constraints of the dark energy. Assuming Gaussianity in the likelihood distribution of the cosmological parameters for the lensing power spectrum [13, 50–53], we utilize a

Fisher matrix analysis [48, 49]:

$$F_{\alpha\beta} = f_{\text{sky}} \sum_l \frac{(2l+1)\Delta l}{2} \text{Tr} \left[\frac{\partial \mathbf{C}_l}{\partial p_\alpha} \tilde{\mathbf{C}}_l^{-1} \frac{\partial \mathbf{C}_l}{\partial p_\beta} \tilde{\mathbf{C}}_l^{-1} \right]. \quad (12)$$

We consider constraints for both a ground-based survey, such as LSST, and a space-based JDEM probe, such as SNAP. We analyze multipoles between 50 and 3000, with the power spectrum of the convergence field divided into multipole bins of width $\Delta l = 50$, (the results are insensitive to the choice of binning). The cutoff at $l = 3000$ avoids non-Gaussianities of the convergence field [13, 50–53], as well as uncertainties from baryonic physics that increase at larger multipoles [15, 16].

We present constraints on cosmology for up to five tomographic bins, where each bin is constructed to contain the same effective number density of galaxies. The redshift divisions of the bins are listed in Table II. For the terms in Eq. 12 we carry out two-sided numerical derivatives with steps of 10% in parameter value (except for ± 0.1 in the case of w_a , and ± 0.05 for Ω_k). Our results are essentially unaffected by the particular choice of step size. We note that there is an ambiguity in the evaluation of the Ω_k derivative at $\Omega_k = 0$, since the Smith et al. fitting functions are only given for flat and open universes. Although it is common to carry out the curvature derivative using the flat cosmology fitting functions, we also evaluate the derivative at a slightly open universe to see if it renders noticeable differences in the constraints. This assumes that the power spectrum doesn’t vary sharply about flatness. The two methods for calculating the Ω_k derivative yield consistent results (within $\sim 15\%$), and we quote results utilizing the latter method.

We consider two dark energy models: $w(z) = w_0 + z/(1+z)w_a$, and $w(z) = w_c$ is constant (i.e., $w_a = 0$). For the w_c case, we define the figure of merit (FOM) of the EOS measurement to be $\text{FOM}(w_c) = \sigma^{-2}(w_c)$. For the $\{w_0, w_a\}$ case, we take the FOM to be the inverse of the error ellipse in the $\{w_0, w_a\}$ plane (as defined in the DETF report [9]):

$$\text{FOM}_{\text{DETF}} = [\sigma(w_p)\sigma(w_a)]^{-1}, \quad (13)$$

where w_p is the pivot value of the EOS. We do not include the factor of $1/\pi$ in the DETF FOM [57]. Note that the uncertainty on the dark energy EOS at the pivot is equal to the uncertainty on a constant EOS [9]. We find that there is roughly a factor of two improvement in $\text{FOM}(w_c)$ in going from Smith et al. to the MTC form for the dark matter power spectrum, as shown in Table III. This relative improvement in the EOS constraint is independent of the number of tomographic bins. Although the derivatives in Eq. 12 are larger for the Smith et al. case (see Fig. 7), the MTC form for the power spectrum provides more stringent constraints due to its reduced cross-correlations in the Fisher matrix. For a 2×2 matrix, this can be visualized as rendering a larger determinant, and thereby

Probe	$\sigma(w_0)$	$\sigma(w_a)$	FOM _{DETF}	$\sigma(w_c)$	FOM(w_c)
1 (M-LSST)	0.51	1.7	1.7	0.34	8.9
2 (M-LSST)	0.14	0.46	80	0.027	1300
3 (M-LSST)	0.082	0.31	190	0.017	3500
4 (M-LSST)	0.071	0.27	240	0.0152	4300
5 (M-LSST)	0.069	0.27	250	0.0148	4600
+ Ω_k	0.15	0.64	96	0.0162	3800
+ Priors	0.072	0.28	230	0.0150	4500
$l < 1000$	0.19	0.81	57	0.022	2100
+ Ω_k	0.23	1.04	36	0.027	1400
+ Priors	0.14	0.59	79	0.022	2200
$z < 1.5$	0.099	0.37	150	0.019	2900
+ Ω_k	0.14	0.74	32	0.043	550
+ Priors	0.010	0.37	140	0.019	2700
+ 2300 SNe	0.043	0.17	410	0.014	4900
1 (S-LSST)	1.4	12	0.16	0.50	3.9
2 (S-LSST)	0.20	0.50	59	0.034	860
3 (S-LSST)	0.082	0.24	170	0.025	1700
4 (S-LSST)	0.069	0.21	220	0.022	2100
5 (S-LSST)	0.067	0.21	230	0.021	2200
$z < 1.5$	0.094	0.29	140	0.025	1600
2 (M-JDEM)	0.22	0.71	31	0.046	480
5 (M-JDEM)	0.11	0.44	100	0.023	1900
+ Ω_k	0.22	0.96	42	0.025	1700
+ Priors	0.11	0.44	98	0.023	1900
$l < 1000$	0.30	1.3	22	0.036	760
+ Ω_k	0.37	1.6	14	0.044	530
+ Priors	0.23	0.95	29	0.036	780
$z < 1.5$	0.15	0.56	58	0.031	1000
+ Ω_k	0.20	1.1	15	0.061	270
+ Priors	0.015	0.56	57	0.031	1000
+ 2300 SNe	0.048	0.21	230	0.021	2200
2 (S-JDEM)	0.32	0.79	21	0.059	280
5 (S-JDEM)	0.11	0.34	87	0.034	860
$z < 1.5$	0.14	0.44	54	0.041	580

TABLE III. FOM values and 1σ constraints on the dark energy parameters, based on either the Smith et al. prescription (denoted by ‘S’) or with the inclusion of MTC corrections (denoted by ‘M’). The +2300 entries in the table are a joint analysis of WL and SNe, with SN systematics included (flatness assumed). The 2300 SNe alone constrain $[w_0, w_a, w_c]$ to $[0.04, 0.67, 0.036]$ in the case of statistical noise only, and to $[0.055, 1.0, 0.054]$ when systematic errors are included. For the cases with priors, we utilize an HST prior of 0.08 on h [55] and a Planck prior of 0.0032 on Ω_k [56]. The strongest improvement comes from the curvature prior.

better constraints as the inverse of the Fisher matrix is taken. Thus, even though smaller derivatives commonly provide poorer constraints, here we find that the cross-correlation terms yield improved constraints for a constant (as well as a redshift-binned) EOS.

Generalizing to non-flat cosmologies significantly degrades the cosmological constraints, especially if we only consider effects out to $z = 1.5$. This degradation is ameliorated with an expected Planck prior of

0.0032 on Ω_k [56] and HST prior of 0.08 on h [55]. For LSST, using the Smith et al. prescription beyond $z = 1.5$, the inclusion of curvature drives the FOM down by one sixth from 4600 to 3800, whereas in the case of a redshift cutoff (at $z = 1.5$) the inclusion of the curvature parameter causes a factor of five deterioration of the dark energy FOM from 2900 to 550. By including HST and Planck priors, the FOM increases to 4500 and 2700, respectively. A similar sensitivity to the curvature density is seen for the JDEM case, which is also effectively removed by our choice of priors. We moreover consider a lower cutoff in l at 1000, noting that this cutoff alone would diminish the constraints by roughly a factor of two for LSST and 2.5 for JDEM. The relative constraint degradation is larger for a JDEM probe as its integrated signal-to-noise is more sensitive to larger multipoles (as seen in Fig. 6).

D. Evolving Dark Energy EOS

One major limitation of the MTC correction to the nonlinear dark matter power spectrum is that it is only valid in the case of a constant dark energy EOS. We now generalize this approach to the case of dynamical dark energy. We utilize an observation by Francis et al. [54], who have shown that the power spectrum of a dynamical $w(z)$ resembles that of a constant w with the same distance to the last scattering surface. In other words, when the integrated expansion history between a dynamical EOS and a constant EOS are similar, the growth histories will likewise be similar. Francis et al. have numerically confirmed this to a few percent, at scales up to $k = 5 h \text{ Mpc}^{-1}$ for the $\{w_0, w_a\}$ parameterization. Based upon this, we mimic the matter power spectrum of an evolving dark energy EOS by utilizing a constant EOS with a matched distance to the last scattering surface. We calculate all other components of the convergence spectrum based upon the actual $w(z)$.

The FOM of the DETF remains relatively unchanged despite the inclusion of the improved (MTC) nonlinear matter power spectrum. For the $\{w_0, w_a\}$ parameterization, we note that although the constraints due to changes in w_0 are improved for MTC, the Smith et al. constraints are more sensitive to changes in w_a , and therefore their net effects on the FOM are roughly equivalent. This latter decrease in sensitivity for MTC occurs as the distance-matching prescription of mapping $\{w_0 = -1, w_a\}$ onto w_c renders larger deviations in the MTC matter power spectrum, and thereby smaller deviations in the convergence spectrum due to the cancellation with the lensing kernel discussed above. The smaller w_a derivatives then lead to inferior constraints. Imposing a cutoff at $l = 1000$ renders a factor of five deterioration in the FOM of the DETF, primarily due to the factor of three deterioration of the constraint on w_a , as shown in Table III.

In addition to the two-parameter $\{w_0, w_a\}$ constraints discussed above, we also consider constraints on a redshift-binned EOS. We utilize the MTC method, generalized following the Francis et al. approach of matching the last-scattering distances between evolving and non-evolving dark energy. Once the weak lensing Fisher matrix for correlated dark energy bins is obtained, we rotate the dark energy parameters into a basis where they are uncorrelated.

The most straightforward approach would be to diagonalize the marginalized Fisher matrix $\tilde{\mathbf{F}}$ (i.e. marginalized over all parameters except for the EOS, $w_{i=1\dots N}$), such that the uncertainties in the uncorrelated dark energy parameters are given by the inverse of the eigenvalues. However, we choose the transformation matrix advocated in Huterer & Cooray (2005) [30], namely $\tilde{\mathbf{F}}^{1/2} = \mathbf{O}^T \mathbf{\Lambda}^{1/2} \mathbf{O}$, where \mathbf{O} and $\mathbf{\Lambda}$ are the eigenvector and eigenvalue matrices. The uncorrelated parameters are then given by $\mathbf{q} = \tilde{\mathbf{F}}^{1/2} \tilde{\mathbf{p}}$ [29, 30, 32, 58]. This transformation matrix has the pleasing feature of generating relatively localized and mostly positive weights [30, 58], while also preserving the information content of the correlated Fisher matrix. Note that the transformation matrix is normalized such that the sum of the elements along each row is equal to unity [30, 58]. The rows therefore represent the contribution of each redshift bin to the decorrelated parameters. The errors on the uncorrelated parameters are then given by

$$\langle \Delta q_i \Delta q_j \rangle = \delta_{ij} \left[\sum_{\alpha} \tilde{F}_{i\alpha}^{1/2} \sum_{\beta} \tilde{F}_{j\beta}^{1/2} \right]^{-1}. \quad (14)$$

We now define the figure of merit for this parameterization to be that of Sullivan, Cooray, & Holz (2007) [31]:

$$\text{FOM}_{\text{wbinned}} = \sum_i \sigma^{-2}(w_i) = \sigma^{-2}(w_c). \quad (15)$$

We note that this FOM is equal to that of a constant EOS [59], which is an important feature as it explicitly demonstrates that the FOM is binning independent. This can be seen by comparing the case of seven bins, $w_{i=1\dots 7}$, with that of one bin, w_c , in Tables III and V. In addition, as the parameter constraints scale as $f_{\text{sky}}^{-1/2}$, both $\text{FOM}_{\text{wbinned}}$ and FOM_{DETF} increase linearly with the fraction of the sky covered.

For comparison with the EOS constraints in Sarkar et al., we have chosen the same redshift binning of the EOS (boundaries at $z = \{0.07, 0.15, 0.3, 0.6, 1.2, 3.0\}$). Although the seventh bin is highly unconstrained, the uncertainty does not leak noticeably into the other parameters (as compared to fixing $w_7 = -1$). This particular binning attempted to maximize the number of redshift bins with 10% or better constraints on the dark energy EOS from future cosmic microwave background (CMB), BAO, and SN data. We have not provided a comparable binning for the case of weak

p_i	(M-LSST)	(M-JDEM)	(S-LSST)	(S-JDEM)
w_c	0.015	0.023	0.021	0.034
FOM	4600	1900	2200	860
Ω_c	0.015	0.028	0.015	0.029
Ω_b	0.015	0.029	0.015	0.029
h	0.11	0.20	0.11	0.20
n	0.016	0.030	0.016	0.031
σ_8	0.0017	0.0028	0.0019	0.0032
w_0	0.069	0.11	0.067	0.11
w_a	0.27	0.44	0.21	0.34
FOM	250	100	230	87
Ω_c	0.015	0.030	0.016	0.029
Ω_b	0.015	0.029	0.015	0.029
h	0.11	0.20	0.11	0.20
n	0.019	0.035	0.016	0.031
σ_8	0.0072	0.011	0.0078	0.012
w_1	0.084	0.12	0.25	0.36
w_2	0.074	0.11	0.31	0.48
w_3	0.036	0.056	0.090	0.14
w_4	0.020	0.031	0.029	0.046
w_5	0.031	0.050	0.034	0.055
w_6	0.41	0.52	0.53	1.5
FOM	4700	1900	2200	870
Ω_c	0.025	0.041	0.048	0.080
Ω_b	0.016	0.029	0.020	0.037
h	0.13	0.22	0.11	0.21
n	0.030	0.047	0.027	0.047
σ_8	0.018	0.027	0.058	0.095

TABLE IV. 1σ uncertainties on cosmological parameters from WL alone, for the case of five tomographic bins in a flat universe without external priors. ‘S’ stands for Smith et al., and ‘M’ for MTC.

lensing. One possible approach is to pick redshifts such that the sensitivity of the integrand to changes in w are equivalent in each bin.

Table IV shows the uncertainties on cosmological parameters for three different EOS parameterizations (w_c , $\{w_0, w_a\}$, and redshift-binned $w(z)$), as determined from weak lensing with five tomographic bins. For a redshift-binned $w(z)$, including the MTC corrections to the dark matter power spectrum, an LSST weak lensing survey constrains five EOS parameters to better than 10% (three of which are better than 5%), and a JDEM-like survey constrains three EOS parameters. The LSST binned FOM is a factor of 2.5 larger than the one for JDEM, and the constraints on other cosmological parameters are roughly a factor of two better. The main point here is that a very wide survey is more effective than a deep, but narrow, survey. Although a deep, moderately wide survey could be even more effective, the constraints depend sensitively on the precise nature of the surveys. The MTC improvement to the nonlinear dark matter power spectrum leads to a factor of two improvement in the FOM

No. of bins	$\sigma(w_1)$	$\sigma(w_2)$	$\sigma(w_3)$	$\sigma(w_4)$	$\sigma(w_5)$	$\sigma(w_6)$	FOM
1 (M-LSST)	0.59	1.47	0.96	0.69	0.74	1.6	8.8
2 (M-LSST)	0.14	0.14	0.074	0.041	0.046	0.30	1300
3 (M-LSST)	0.099	0.085	0.043	0.024	0.032	0.53	3600
4 (M-LSST)	0.082	0.075	0.038	0.020	0.031	0.47	4500
5 (M-LSST)	0.084	0.074	0.036	0.020	0.031	0.41	4700
+ Ω_k	0.080	0.072	0.037	0.021	0.041	0.13	3900
+ Priors	0.083	0.074	0.037	0.020	0.032	0.33	4600
$l < 1000$	0.12	0.10	0.052	0.029	0.050	0.16	2200
+ Ω_k	0.13	0.11	0.060	0.035	0.075	0.20	1400
+ Priors	0.13	0.10	0.052	0.028	0.049	0.19	2200
$z < 1.5$	0.11	0.10	0.045	0.024	0.043	1.4	3000
+ Ω_k	0.20	0.18	0.088	0.052	0.40	0.52	560
+ Priors	0.12	0.10	0.046	0.025	0.046	1.27	2700
+ 2300 SNe	0.055	0.049	0.032	0.021	0.032	0.50	5000
1 (S-LSST)	0.56	2.8	2.2	2.1	2.5	17	3.9
2 (S-LSST)	0.29	0.90	0.25	0.065	0.043	0.17	850
3 (S-LSST)	0.33	0.40	0.12	0.037	0.035	0.43	1700
4 (S-LSST)	0.22	0.29	0.095	0.031	0.034	0.57	2100
5 (S-LSST)	0.25	0.31	0.090	0.029	0.034	0.53	2200
$z < 1.5$	0.26	0.28	0.087	0.032	0.047	1.0	1600
2 (M-JDEM)	0.22	0.22	0.12	0.067	0.082	0.52	490
5 (M-JDEM)	0.12	0.11	0.056	0.031	0.050	0.52	1900
+ Ω_k	0.12	0.11	0.056	0.032	0.062	0.22	1700
+ Priors	0.12	0.11	0.056	0.031	0.051	0.49	1900
$l < 1000$	0.20	0.17	0.086	0.048	0.085	0.26	790
+ Ω_k	0.22	0.18	0.097	0.056	0.12	0.32	550
+ Priors	0.21	0.17	0.086	0.047	0.081	0.30	810
$z < 1.5$	0.18	0.16	0.073	0.040	0.078	1.7	1100
+ Ω_k	0.27	0.26	0.13	0.075	0.67	0.75	270
+ Priors	0.18	0.16	0.073	0.040	0.079	1.6	1000
+ 2300 SNe	0.067	0.061	0.045	0.033	0.056	0.58	2200
2 (S-JDEM)	0.45	1.3	0.43	0.11	0.075	0.29	280
5 (S-JDEM)	0.36	0.48	0.14	0.046	0.055	1.5	870
$z < 1.5$	0.36	0.45	0.14	0.052	0.082	1.5	580

TABLE V. 1σ constraints on values of $w(z)$ in uncorrelated redshift bins, where ‘S’ stands for Smith et al., and ‘M’ for MTC. The EOS is redshift binned at $z = \{0.07, 0.15, 0.3, 0.6, 1.2, 3.0\}$, but decorrelating the covariance matrix for the original bins results in a leakage across bins. Figure 8 shows this leakage in terms of window functions. The 2300 SNe alone constrain the six EOS bins to $[0.11, 0.10, 0.12, 0.69, 0.24, 1.2]$.

of a redshift-binned EOS.

It is possible to compare our weak lensing constraints with the combined constraints from SNe, BAOs, and CMB. The latter have been calculated in Sarkar et al. [32], using a Markov Chain Monte Carlo (MCMC) likelihood approach. Case C in Sarkar et al. considers a mock catalog of 300 SNe at $z < 0.1$ [60] and 2000 SNe in the range of $0.1 < z < 1.8$ [44], two current BAO distance estimates [61, 62], fifteen optimistic future BAO measurements (five from V1N1 of [63], ten from ADEPT [64]), as well as CMB constraints on $[\Omega_m h, h, R]$ of $[0.023, 0.08, 0.03]$ [55, 65,

66], where R is the distance to the last scattering surface. For this extensive data set, the redshift-binned dark energy FOM is 1300. In comparison, our projected lensing constraints yield an FOM of 4700 for LSST and 1900 for JDEM (for the MTC matter power spectrum). It is evident that weak lensing is potentially an extraordinarily powerful dark energy probe.

E. SN/Weak Lensing Complementarity

Our distribution of lensing source galaxies peaks at a redshift of unity. It is therefore interesting to combine our higher-redshift lensing measurements with those from supernovae. To this end, we uniformly distribute a set of 300 SNe at $z < 0.1$ [60], and 2000 SNe in the range $0.1 < z < 1.8$ (as expected from a space-based JDEM probe [44], or as part of a first data release by a ground-based telescope such as LSST). For each supernova we take the intrinsic noise to be a Gaussian in magnitude with $\sigma_{\text{int}} = 0.1$ [67]. We divide the Hubble diagram for $z > 0.1$ into 50 redshift bins, and associate each bin with a redshift-dependent systematic floor of magnitude $\delta_m = 0.02(0.1/\Delta z)^{1/2}(1.7/z_{\text{max}})(1+z)/2.7$ [68]. We assume that this irreducible systematic has no correlation between bins. For the SN constraints we use an HST prior of 0.08 for h [55] (which is also applied to the WL case in the comparison with SNe+WL). For further details on the SN approach we refer the

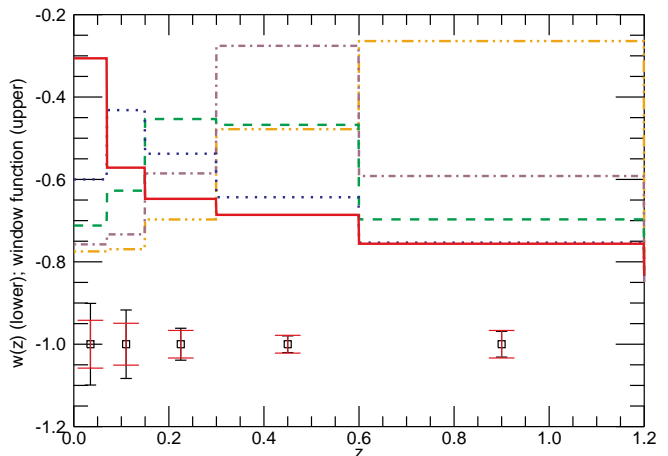


FIG. 8. Lower portion of the figure shows the constraint on the dark energy EOS in five redshift bins. The narrow (black) error bars are obtained from weak lensing alone, for five tomographic bins, with an HST prior on the Hubble constant. The wide (red) error bars are obtained from a joint analysis of WL and SNe. Note that we are neglecting WL systematic uncertainties in this plot. The upper half of the figure illustrates the window functions associated with the first five decorrelated dark energy bins (WL + SNe). (Note that the window functions have been shifted down by a constant of 0.8 for visual clarity.)

Probe	$ \delta(w_0) $	$ \delta(w_a) $	FOB(w_0, w_a)	$ \delta(w_c) $	FOB(w_c)	
LSST	0.073	0.19	1.9	0.026	1.8	
JDEM	0.076	0.20	1.3	0.027	1.2	
Probe	$ \delta(w_1) $	$ \delta(w_2) $	$ \delta(w_3) $	$ \delta(w_4) $	$ \delta(w_5) $	$ \delta(w_6) $
LSST	0.0050	0.060	0.080	0.034	0.0026	0.029
JDEM	0.0039	0.20	0.18	0.058	0.0069	0.031

TABLE VI. Bias on the determination of the dark energy equation of state, for the case of five tomographic bins (in a flat universe with no external priors). For the FOB of $\{w_0, w_a\}$, a value of 1.5 indicates a 1σ shift from the true estimate, and a value of 2.5 indicates a 2σ shift [23, 70]. For w_c , these values are 1.0 and 2.0, respectively. The lower entries list the bias on the *correlated* $w(z)$ bins.

reader to earlier work [32].

The uncorrelated redshift-bin uncertainties in five tomographic weak lensing bins are given in Tables IV and V, and illustrated in Figure 8 for an LSST data set. The narrow (black) error bars are the constraints from weak lensing alone, while the wide (red) error bars represent the constraints from both weak lensing and SNe. Although weak lensing alone constrains three redshift bins to 5%, by combining this data set with SNe we constrain two additional EOS parameters to that level. Weak lensing and SNe are complementary, as weak lensing is most effective for constraints at intermediate redshifts (roughly $0.2 < z < 1.2$), while future SN data provide a more effective probe at lower redshifts ($z < 0.2$).

F. Bias in dark energy due to uncertainties in the nonlinear matter power spectrum

We have calculated the improvement in weak lensing constraints from use of the MTC matter power spectrum (incorporating $w(z) \neq -1$). It is also interesting to calculate the bias that would arise from use of the more approximate Smith et al. power spectrum, when the real data is described by MTC. The bias in each parameter is given by [23, 69]:

$$\delta p_\alpha = f_{\text{sky}} \sum_{l,\beta} F_{\alpha\beta}^{-1} \frac{(2l+1)\Delta l}{2} \text{Tr} \left[\tilde{\mathbf{C}}_l^{-1} \frac{\partial \mathbf{C}_l}{\partial p_\beta} \tilde{\mathbf{C}}_l^{-1} \delta C_l \right], \quad (16)$$

where δC_l is the difference between the MTC and Smith et al. convergence spectra. One can calculate the corresponding figure of bias (FOB) for the subset of EOS parameters as rendered by [23]:

$$\text{FOB} = \left(\sum_{\alpha,\beta} \delta p_\alpha \tilde{F}_{\alpha\beta} \delta p_\beta \right)^{1/2}. \quad (17)$$

Thus, for the case of one parameter, the FOB is simply equal to the ratio of that parameter's bias to its uncertainty. Table VI presents the FOB values for LSST

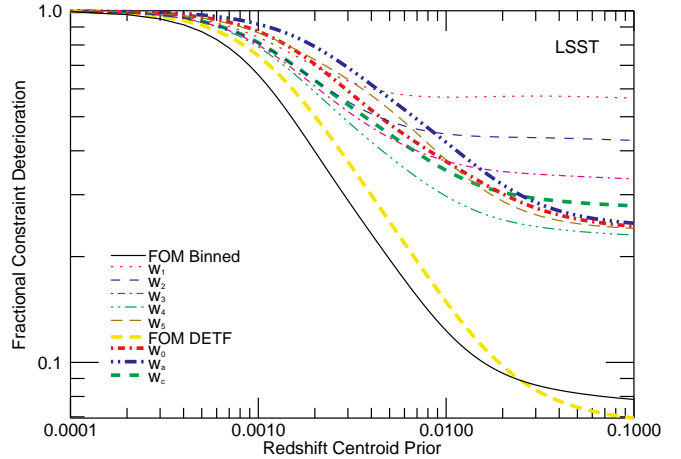


FIG. 9. Deterioration of constraints as a function of a Gaussian prior on each centroid of the redshift bins for LSST. We plot both $\text{FOM}_{\text{sys}+\text{prior}}/\text{FOM}_{\text{no-syst}}$ and $\sigma(w)|_{\text{no-syst}}/\sigma(w)|_{\text{sys}+\text{prior}}$.

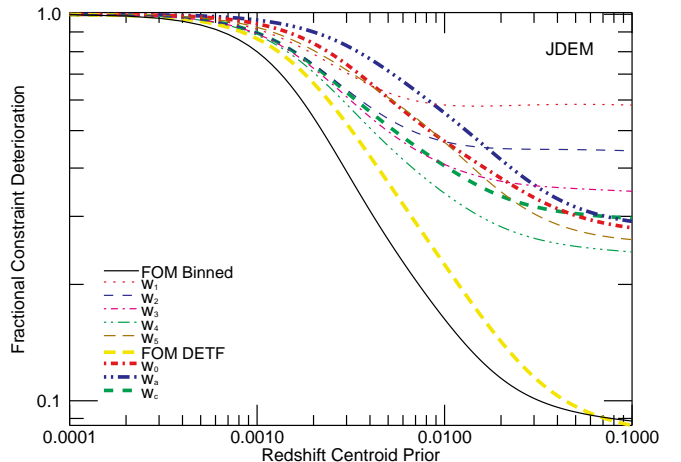


FIG. 10. Deterioration of constraints as a function of the prior on the centroid of the redshift bins for a JDEM survey.

and JDEM weak lensing measurements. We find a 1σ – 2σ bias between the Smith et al. and MTC determinations of the dark energy EOS (for a $w = -0.9$ fiducial cosmology). *It is therefore critical that the nonlinear matter power spectrum be well-characterized, to enable precision constraints on a dynamical dark energy equation of state.*

G. Systematic Uncertainties

To assess the importance of systematic errors in the weak lensing measurements, we approximate a possible shear miscalibration by including a multiplicative factor, f_i , for each tomographic bin. We ignore additive systematic terms to the convergence power spectrum, as their dependence on l is currently poorly

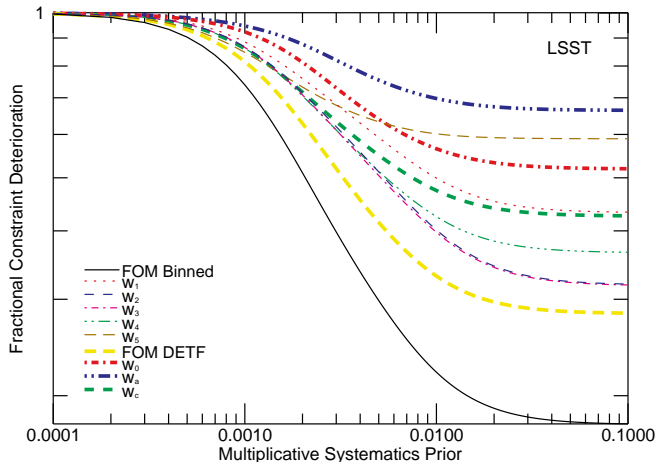


FIG. 11. Deterioration of constraints as a function of the Gaussian prior on each multiplicative factor in shear for LSST.

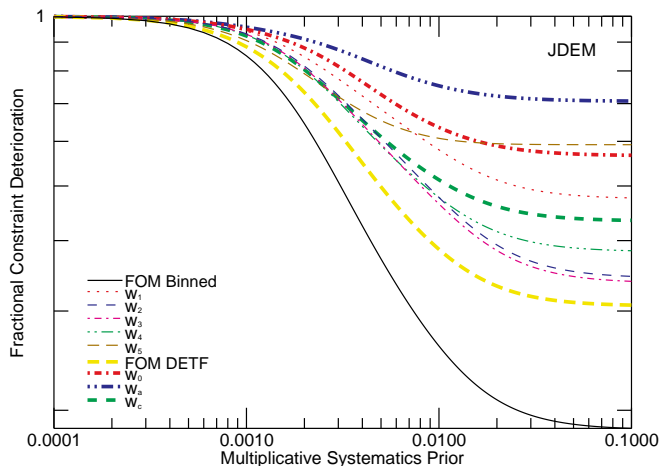


FIG. 12. Deterioration of constraints as a function of the prior on multiplicative factors in shear for a JDEM survey.

understood [71]. The uncertainty in the redshift distribution of the sources is modeled to first order as a shift in the centroid of the tomographic bins [11]. We ignore other possible sources of systematics, such as baryonic uncertainties in the nonlinear scales of the matter power spectrum [14], and intrinsic ellipticity correlations of the source galaxies [12].

Following Huterer et al. (2006) [11], the cross-correlation terms are changed by the systematics as: $C_{ij}(l) = C_{ij}(l; z_i + \delta z_i, z_j + \delta z_j) [1 + f_i + f_j]$. For our five tomographic bins we therefore introduce an additional $5 \times 2 = 10$ free parameters to encapsulate possible systematics. The effect of these systematic uncertainties on the measurement of dark energy is heavily influenced by the corresponding priors. If we are optimistic, and claim an understanding of the systematics at the 0.1% level, the deterioration in dark energy constraints is essentially negligible. However, the constraints are strongly compromised if the sys-

tematics are unknown at the level of 1%. This is illustrated in Figures 9–12.

Both of the surveys offer the potential for self-calibration tests, if the priors are above the percent level. For LSST, there is a factor of five (three) degradation of the binned FOM (DETF FOM) for multiplicative shear errors and a factor of 14 deterioration in the two FOMs for errors in the redshift bin centroids. In general the degradations are slightly milder for JDEM; e.g. a factor of 11 degradation in the two FOMs for redshift bin centroid uncertainties. We note that a combined analysis with the lensing bispectrum has the potential to improve these prospects [11].

IV. CONCLUSIONS

We calculate weak lensing constraints on the dark energy equation of state, incorporating an improved nonlinear matter power spectrum which accounts for the effects of a dynamical dark energy. The most commonly utilized nonlinear extension of the matter power spectrum, calibrated from N-body simulations by Smith et al., does not incorporate the effects of time-evolving dark energy. We follow a prescription presented by McDonald, Trac, & Contaldi (2006), and extend the Smith et al. form to include evolving dark energy. We then perform a full Fisher matrix analysis for two prospective weak lensing surveys, utilizing the improved power spectrum.

By considering weak lensing tomography with an improved nonlinear matter power spectrum that incorporates dynamical dark energy, we find a factor of two improvement in the dark energy figure of merit (for the WMAP5 fiducial cosmology). Although the changes in the matter power spectrum and the lensing kernel somewhat cancel in their effects on the convergence power spectrum, the parameter correlations nonetheless lead to improved parameter constraints.

We further show that a poor approximation (off by $\gtrsim 10\%$) to the dark energy corrections of the nonlinear matter power spectrum leads to a $\gtrsim 1\sigma$ bias on the dark energy equation of state. Future weak lensing surveys must therefore incorporate percent-level accurate dark energy modifications to the nonlinear matter power spectrum to avoid introducing significant bias in their measurements. In addition, by combining weak lensing data with supernova measurements at lower redshifts, we show that a general dark energy model can be constrained in five redshift bins to 5% for an LSST-type survey and to 10% for a JDEM-like probe. These dark energy constraints are contingent upon our ability to understand weak lensing systematic uncertainties, such as those arising from shear miscalibration and the redshift uncertainty of the sources. If it is possible to control these systematics to 0.1%, weak lensing constraints of dynamical dark energy from next-generation surveys offer tremendous promise.

Acknowledgments: We are grateful to Alexandre Amblard and Paolo Serra for helpful conversations throughout this work. We also thank Dragan Huterer, Patrick McDonald, Charles Shapiro, and Licia Verde

for useful discussions. S.J. acknowledges support from a GAANN fellowship at UCI. This work was also supported by NSF CAREER AST-0645427 (A.C.) and LANL IGPP Astro-1603-07 (D.E.H.).

-
- [1] Refregier, A., *Ann. Rev. Astron. Astrophys.*, **41**, 645 (2003).
- [2] Bartelmann, M., Schneider, P., *Phys. Rept.*, **340**, 291 (2001).
- [3] Wittman, D. M., et al., *Nature*, **405**, 143 (2000).
- [4] Kaiser, N., Wilson, G., Luppino, G. A., arXiv:astro-ph/0003338v1 (2000).
- [5] Bacon, D., Refregier, A., Ellis, R., *MNRAS*, **318**, 625 (2000).
- [6] van Waerbeke, L., et al., *A&A*, **358**, 30 (2000).
- [7] Jarvis, M., et al., *Astrophys. J.*, **644**, 71 (2006).
- [8] Hoekstra, H., et al., *Astrophys. J.*, **647**, 116 (2006).
- [9] Albrecht, A., et al., arXiv:astro-ph/0609591 (2006).
- [10] Ma, Z., Hu, W., Huterer, D., *Astrophys. J.*, **636**, 21 (2005).
- [11] Huterer, D., et al., *MNRAS*, **366**, 101 (2006).
- [12] Hirata, C. M., Seljak, U., *Phys. Rev. D*, **70**, 063526 (2004).
- [13] Scoccimarro, R., Zaldarriaga, M., Hui, L., *Astrophys. J.*, **527**, 1 (1999).
- [14] Huterer, D., Takada, M., *Astropart. Phys.*, **23**, 369 (2005).
- [15] White, M., *Astropart. Phys.*, **22**, 211 (2004).
- [16] Zhan, H., Knox, L., *Astropart. Phys.*, **616**, L75 (2004).
- [17] Rudd, D., Zentner, A. R., Kravtsov, A. V., *Astrophys. J.*, **672**, 19 (2008).
- [18] Huterer, D., *Phys. Rev. D*, **65**, 063001 (2002).
- [19] McDonald, P., Trac, H., Contaldi, C., *MNRAS*, **366**, 547 (2006).
- [20] Cooray, A., Hu, W., *Astrophys. J.*, **574**, 19 (2002).
- [21] Shapiro, C., Cooray, A., *JCAP*, **03**, 007 (2006).
- [22] Hirata, C., Seljak, U., *Phys. Rev. D*, **68**, 083002 (2003).
- [23] Shapiro, C., arXiv:0812.0769v1 (2008).
- [24] Dodelson, S., Shapiro, C., White, M., *Phys. Rev. D*, **73**, 023009 (2006).
- [25] Smith, R. E., et al., *MNRAS*, **341**, 1311 (2003).
- [26] Dunkley, J., et al., *Astrophys. J. Suppl.*, **180**, 306 (2009).
- [27] Linder, E. V., *Phys. Rev. Lett.*, **90**, 091301 (2003).
- [28] Chevallier, M., Polarski, D., *Int. J. Mod. Phys.*, **D10**, 213 (2001).
- [29] Huterer, D., Starkman, D., *Phys. Rev. Lett.*, **90**, 031301 (2003).
- [30] Huterer, D., Cooray, A., *Phys. Rev. D*, **71**, 023506 (2005).
- [31] Sullivan, S., Cooray, A., Holz, D., *JCAP*, **09**, 004 (2007).
- [32] Sarkar, D., et al., *Phys. Rev. Lett.*, **100**, 241302 (2008).
- [33] Song, Y.-S., Knox, L., *Phys. Rev. D*, **70**, 063510 (2004).
- [34] Linder, E. V., Jenkins, A., *MNRAS*, **346**, 573 (2003).
- [35] Hu, W., *Astrophys. J.*, **522**, L21 (1999).
- [36] Zhan, H., Knox, L., Tyson, J. A., *Astrophys. J.*, **690**, 923 (2009).
- [37] <http://www.lsst.org>
- [38] Ivezić, Z., et al., arXiv:0805.2366v1 (2008).
- [39] D. Limber, *Astrophys. J.* **119**, 655 (1954).
- [40] Jain, B., Seljak, U., *Astrophys. J.*, **484**, 560 (1997).
- [41] Cooray, A., Hu, W., Miralda-Escude, J., *Astrophys. J.*, **535**, L9 (2000).
- [42] Takada, M., Jain, B., *MNRAS*, **348**, 897 (2004).
- [43] <http://universe.nasa.gov/program/probes/jdem.html>; <http://snap.lbl.gov>.
- [44] Aldering, G., et al., arXiv:astro-ph/0405232v1 (2004).
- [45] Refregier, A., et al., *Astron. J.*, **127**, 3102 (2004).
- [46] Cooray, A., Sheth, R. K., *Phys. Rept.*, **372**, 1 (2002).
- [47] Eisenstein, D. J., Hu, W., *Astrophys. J.*, **511**, 5 (1997).
- [48] Hu, W., Jain, B., *Phys. Rev. D*, **70**, 043009 (2004).
- [49] Tegmark, M., *Phys. Rev. Lett.*, **79**, 3806 (1997).
- [50] White, M., Hu, W., *Astrophys. J.*, **537**, 1 (2000).
- [51] Cooray, A., Hu, W., *Astrophys. J.*, **554**, 56 (2001).
- [52] Takada, M., Jain, B., arXiv:0810.4170v1 (2008).
- [53] White, M., Hu, W., *Astrophys. J.*, **554**, 67 (2001).
- [54] Francis, M. J., Lewis, G. F., Linder, E. V., *MNRAS*, **380**, 1079 (2007).
- [55] Freedman, W., et al., *Astrophys. J.*, **553**, 47 (2001).
- [56] Smith, K. M., Hu, W., Kaplinghat, M., *Phys. Rev. D*, **74**, 123002 (2006).
- [57] Albrecht, A., et al., arXiv:0901.0721v1 (2009).
- [58] Hamilton, A. J. S., Tegmark, M., *MNRAS*, **312**, 285 (2000).
- [59] de Putter, R., Linder, E. V., *Astropart. Phys.*, **29**, 424 (2008).
- [60] Aldering, G., et al., *Proc. SPIE*, **4836**, 61 (2002).
- [61] Eisenstein, D. J., et al., *Astrophys. J.*, **633**, 560 (2005).
- [62] Percival, W. J., et al., *MNRAS*, **381**, 1053 (2007).
- [63] Seo, H.-J., Eisenstein, D. J., *Astrophys. J.*, **598**, 720 (2003).
- [64] Riess, A., (private communication).
- [65] Tegmark, M., et al., *Astrophys. J.*, **606**, 702 (2004).
- [66] Wang, Y., Mukherjee, P., *Phys. Rev. D*, **76**, 103533 (2007).
- [67] Kim, A. G., et al., *MNRAS*, **347**, 909 (2004).
- [68] Linder, E. V., Huterer, D., *Phys. Rev. D*, **67**, 081303 (2003).
- [69] Knox, L., Scoccimarro, R., Dodelson, S., *Phys. Rev. Lett.*, **81**, 2004 (1998).
- [70] Press, W. H., et al., *Numerical recipes: the art of scientific computing* (3rd ed.), Cambridge Univ. Press, (2007).
- [71] Hannestad, S., Tu, H., Wong, Y., *JCAP*, **06**, 025 (2006).